Quantifying Intracellular Mechanosensitive Response upon Spatially Defined Mechano-Chemical Triggering

Elaheh Zare-Eelanjegh[a,1], Renard T.M. Lewis[b], Ines Lüchtefeld[a], Ulrike Kutay[b], Tomaso Zambelli[a,1]

[a] Laboratory of Biosensors and Bioelectronics, Institute for Biomedical Engineering, ETH Zurich, Zurich, Switzerland
[b] Department of Biology, Institute of Biochemistry, ETH Zurich, Zurich, Switzerland.

[1] To whom correspondence may be addressed. Email: ztomaso@ethz.ch or elaheh.zare@alumni.ethz.ch

Author contributions: E.Z.E., R.T.L., U.K., and T.Z. designed research; E.Z.E., I.L. and R.T.L. performed experiments and analyzed data; and E.Z.E. and R.T.L. wrote the paper.

Keywords: Mechanotransmission, nuclear mechanoresponse, endoplasmic reticulum mechanoresponse, tension, lamins, cytoskeleton

Abstract

The mechanotransduction process relies on the interaction of mechanical and biochemical cues, transmitting cellular forces to intracellular organelles to activate biochemical pathways and elicit responses. This involves mechanoresponsive components like actin filaments, microtubules (MTs), and the lamin meshwork. Fluidic force microscopy (FluidFM), a force-controlled micropipette allows for the manipulation of intact cells mechanically and chemically, providing a novel approach to study mechanotransmission in cells *in situ*. FluidFM combined with fluorescence lifetime imaging microscopy (FLIM), enables high-resolution mapping of intracellular tension dynamics. Here, we used cells with varying nuclear lamina compositions to explore the lamina's role in initiating mechanoresponse to external cues. We found that A-type and B-type lamins trigger nuclear mechanoresponse distinctly, with A-type lamins contributing to nuclear elasticity, whereas B-type lamins influence viscous response. Moreover, MTs underwent mechanical adaptation and assisted in releasing the tension in lamin A/C knockout (KO) cells, contrasting with healthy cells where MTs aid to preserve the tension locally rather than transferring it. This research provides insights into the dynamic mechanoresponse of cellular components and supports targeted therapies for mechanical stress-related diseases.

Introduction

Mechanical forces regulate cell behavior and function. The cytoskeleton, particularly the actinomyosin network, acts as a primary receptor and transmitter of these signals.[1,2] Biological tissues and organs are influenced by these mechanical signals at the cellular level.[3]

Moreover, cells coordinately transmit external forces into the intracellular organelles, activate biochemical pathways, and eventually elicit corresponding cellular responses.[4,5] This relies on interconnected mechanosensory systems, including ion channels, membrane receptors, cytoskeletal components, and the Linker of Nucleoskeleton and Cytoskeleton (LINC) complex that bridges the cytoskeleton to the nucleus.[6] Additionally, the nucleus, a major mechanosensitive organelle, can directly sense large-scale forces resulting in nuclear deformations and gene expression changes via a process called 'nuclear mechanotransduction'.[7] Other organelles such as the endoplasmic reticulum (ER)[8], mitochondria[9] and Golgi apparatus[10] can also sense transmitted forces. The nuclear lamins, intermediate filaments lining the inner side of inner nuclear membrane, likely collaborate with the LINC to regulate nuclear tension and mechanotransduction.[11,12] Forces convert into biochemical cues at the nuclear envelope through phosphorylation of lamin A and emerin, a mechanosensitive inner nuclear membrane (INM) protein that associates with lamin A/C.[13] The general belief is that viscoelastic responses of the nucleus to physiological forces are governed by the interactions between A- and B-type lamins as well as chromatin.[14] Understanding the mechanical roles of lamin A/C and lamins B1/B2 will enhance our knowledge of nuclear deformation in health and disease. Notably, different mechanotransduction pathways crosstalk and interplay with biochemical signals (*e.g.*, growth factors) to elucidate specific cell behaviors.[15] Disruption of biomechanical homeostasis and failure of cells to appropriately transmit the mechanical stimuli into the requisite biochemical pathways, can lead to diseases such as arthritis, atherosclerosis, and cancer.[16,17]

Several methods have been developed to explore single cell mechanics and mechanotransmission including atomic force microscope (AFM), optical tweezer (OT), magnetic tweezer (MT), biomembrane force probes (BFP), traction force microscope (TFM), optogenetic mechanostimulators and DNA-based mechanical sensors.[18,19] Recently, a time-shared optical tweezer microrheology method (TimSOM) that measures viscoelastic properties of cytoplasm, nuclear envelope, and nucleoplasm in living systems has been reported.[20] However, these methods often face limitations in measuring intracellular forces at the molecular level within the cell's natural state.[21] For instance, the recently developed TimSOM requires embedding tracer beads inside cells or embryos and yields averaged measurements over small regions rather than pinpointing single molecular-scale forces. To overcome such constrains, FRET[22,23] and FLIM-based[24,25] tension sensors have been engineered for studying intracellular mechanosensing at the molecular level. FRET detects energy transfer between two fluorophores in proximity, indicating molecular interactions and conformational changes within biological systems. Unlike intensity-based FRET methods, FLIM measures the lifetime of fluorescent molecules excited by a laser pulse, offering a quantitative signal

for molecular interactions independent of reporter molecule concentration. To delve into the interplay of biochemical and mechanical aspects in cellular behaviors, we require tools that can sensitively stimulate living cells both mechanically and chemically in their natural state, while observing intracellular dynamics. Furthermore, these methods should quantify minute forces with superior spatial and temporal resolution.

Fluidic force microscopy (FluidFM), a micropipette configured on an AFM, addresses this challenge.[26] The FluidFM micro channeled-cantilever with a nano-aperture, connected to a fluidic pressure controller, enables quantitative injection of impermeable molecules into subcellular compartments of living cells.[27-30] such injections can be realized as biochemical triggering of the cellular events with spatial and temporal resolution while preserving cell viability. Combining FluidFM with optical readouts like FLIM-based molecular sensor enables simultaneous manipulation of intact cells and quantifying their responses.

In this work, we first used FluidFM combined with the FLIM for *in situ* mechanical (*i.e.*, indentation) and chemical (*i.e.*, drug injection) triggering of cells with simultaneous intracellular tension mapping at the nuclear envelope and ER. Further, mechanoresponsive crosstalk between different organelles within the cell including the nucleus, ER and cytoskeleton. For chemical interference, we injected cytochalasin D (CytoD) and/or nocodazole (Noco) to inhibit the actin and/or microtubule network, respectively. Next, we exploited cell lines in which nuclear lamins were perturbed (*i.e.*, wild-type HeLa (WT), lamin A/C gene (*LMNA)* KO, *LMNB1* and *LMNB2* (LMNB)-knockdown (KD) and *LMNA* KO+LMNB-KD and subjected to mechano-chemical stimulation and quantification of tension changes.

Results and discussion

We had previously reported the development of a FluidFM-FLIM system based on a customized stage for mounting our AFM head on top of a confocal inverted microscope to investigate the effect of the plasma membrane tension on the opening of mechanosensitive ion channels.[31] Here, we used HeLa cells stained with ER Flipper-TR, a tension reporter dye which selectively labels the ER and nuclear membrane constituting a continuous membrane network.[24] ER Flipper-TR measures the membrane tension changes through alterations in its fluorescence lifetime and serves as a quantitative readout for the tension responses to the external stimuli within living cells. FLIM signals were recorded before, during and after the mechanical or mechano-chemical stimulus facilitated by FluidFM.

Mechanical stimulation of the nucleus: impact of probe apex shape on cellular mechanoresponse.

The geometry of an AFM probe determines how a force is spatially applied on a cell surface.[32] Different probe shapes cause varying membrane deformations, activating diverse mechanoresponses through mechanical involvement of various organelles. The cellular cytoskeleton plays crucial roles in distributing and absorbing mechanical forces to maintain cellular integrity and function. Cylindrical and pyramidal FluidFM probes were used for indenting and puncturing the nucleus under varied forces (Fig. 1 A and B). Cylindrical FluidFM probes were sharpened using a focused ion beam (FIB) to facilitate membrane rupture with minimal stress (Fig. 1B, see Methods section). In parallel, Lifetime images of ER Flipper-TR stained HeLa cells were obtained using a FLIM detector integrated into a confocal laser scanning microscope (Fig. 1C). The images, color-coded for clarity, report the conformational shifts in the ER Flipper-TR molecule. Higher lifetime values (red color) indicate increased membrane tension.

Subsequently, different “Region of Interests” (ROIs) were manually selected for the ER, nuclear membrane (Nuc-mem), and the area around the indentation site (Indent-site) (*SI Appendix*, Fig. S1 and Fig. 1C middle) and their lifetime values were analyzed. Mean lifetime values within each ROI were normalized by subtracting the initial values for each cell (see *SI Appendix* and Fig 1D). The average lifetime values at the ER showed greater tension increase with pyramidal probes compared to cylindrical probes across a range of indentation forces (10 - 100 nN) (Fig. 1D, top left). The ER retains this higher tension even after retracting the probe and removal of the external mechanical stimulus (Fig. 1D, bottom left). At the nuclear envelope (NE), both pyramids and cylinders impose the same amount of stress during mechanical stimulus (Fig. 1D, top middle). Yet, following the removal of the probe terminating the mechanical perturbation, pyramidal probes reveal increased tension at NE at higher indentation forces of 50 nN and 100 nN in contrast to the cylinders (Fig. 1D, top middle). At the NE, a decrease in lifetime or relaxation in tension occurred between 10 nN and 50 nN indentation, observed only with cylindrical probes. Since this is within the expected range of indentation force during membrane rupture, the observed relaxation in tension is related to membrane rupture and cylinder insertion in HeLa cells. Although pyramidal probes are also expected to puncture the cell membrane and subsequently the NE upon indenting cells targeting their nucleus with increasing forces

117 (*i.e.*, around 100 nN for HeLa cells[28]), their insertion phenomena within the membranes is not instantaneous
118 and thus not detectable within the graph demonstrating the quantified tension upon indentation (Fig. 1D,
119 top middle). Sharpened cylindrical probes elicit higher tension locally at the indentation site when compared
120 to pyramids during indentation (Fig. 1D, top right). This is due to the cylindrical geometry leading to a smaller
121 area where the inserting force is employed, increasing the pressure locally, while minimizing the
122 disturbance to other organelles such as the ER. Hence, sharpened cylindrical probes exert a lower overall
123 tension on the cells during injection. Immediately following the retraction of cylindrical probes, the tension
124 remains constant or slightly reduces. But, for pyramidal probes, surprisingly, the lifetime increases within
125 all ROIs immediately following the retraction. This suggests an additional mechanical stress upon the
126 withdrawal of pyramidal probes.

127 Lastly, to assess the origin of higher tension imposed locally by cylindrical probes compared to pyramidal
128 ones, the deformation of cell nuclei was quantified during the indentation process using lateral images
129 acquired by the confocal microscopy (Fig. 1E). For this, FluidFM probes were filled with sulforhodamine
130 (SuR) dye (red) and the nuclei, stained with Hoechst (blue) were subjected to indentation at varied forces
131 while acquiring z-stacks images before and during stimulus. Then, the lateral views were obtained from z-
132 stack images, and the nucleus perimeter was measured before and during indentation for both pyramidal
133 and cylindrical probes (Fig. 1F). As expected, cylinders introduce higher deformation of cell nuclei with
134 maximum deformation around the apex (Fig. 1E). This rationalizes the higher lifetime values reported for
135 the indentation site for cylinders compared to pyramids (Fig. 1D, top right).

136 Collectively, the use of different probe shapes for mechanical stimulation of the nucleus revealed a distinct
137 tension distribution across varied subcellular compartments. While tension was higher around the
138 cylindrical probe, a higher tension at the ER was observed when pushing with a pyramidal probe. This could
139 be attributed to the greater total volume displacement caused by the broader apex of pyramidal probes
140 compared to the sharper tips of cylindrical ones. Furthermore, tension was increased in the ER and the NE
141 of cells stimulated by the pyramids upon removal of probes, which was not the case for the cylinders. Since
142 the cytoskeleton is essential for sensing such mechanical stimuli and for the downstream responses (*e.g.*,
143 transcription), we further explored whether chemically induced depolymerization of actin filaments affects
144 the response of cells to mechano-stimulation, combining nucleus indentation and CytoD injection.

145 Disrupting actin filament dynamics by mechano-chemical triggers inhibits their active support of 146 the stressed nucleus.

147 The dynamics of cytoskeletal and nuclear actin, whether in monomeric (G-actin) or filamentous (F-actin)
148 forms, affects both the sensing and response to mechanical stimuli, as well as the resulting transcriptional
149 processes.[33,34] The mechanosensitive LINC complex in tandem with cytoskeletal components regulates
150 nuclear function and protects the nucleus from excessive mechanical stress. CytoD disturbs actin filament
151 dynamic mainly by binding to G-actin and inhibiting filament assembly.[35] We investigated whether CytoD
152 interruption of the actin network alters the tension load on the nucleus, thus modifying the nuclear

153 mechanoresponse. Therefore, actin filaments were chemically disrupted by a mechano-chemical
154 stimulation through indenting the nucleus and concurrently injecting CytoD in a spatio-temporally defined
155 fashion (Fig. 2 A and B). Since CytoD is smaller in size than the passive diffusion limit of nuclear pore
156 complexes, it distributes throughout the nucleus and cytosol, interacting with both nuclear and cytoskeletal
157 actin, thereby influencing overall cell structure and its mechanoresponsive behavior. While CytoD is
158 believed to permeate cell membranes, its active intracellular injection allows for real-time tracking of
159 dynamic responses. Additionally, when quantitatively injected, the amount taken up by different cells is
160 consistently controlled, regardless of variations in cell responses.

161 FluidFM probes were filled with 50 µM CytoD in DMSO (or DMSO for control groups) and used for mechano-
162 chemical triggering by indenting the nucleus at 150 nN ("mech"), followed by a quantitative intracellular
163 injection of CytoD or DMSO ("mech + inj") (Fig. 2 A and B). The indentation force was adjusted to 150 nN
164 to ensure a successful injection into HeLa cells. FLIM measurements were performed before, during "mech"
165 and "mech + inj", and just after the manipulation (Fig. 2 B and C). Indentation force applied by AFM, serving
166 as a controlled mechanical stimulus (black line), fluidic pressure pulse used for injection (orange line), and
167 time-lapse lifetime values recorded by the FLIM detector (dark blue crosses and light blue fitted curve) were
168 recorded simultaneously (Fig. 2B). This injection process delivers ~10 fL of CytoD (or DMSO), equivalent
169 to ~1% of the cell's volume, leading to a final intracellular concentration of 0.5 µM. During "mech + inj", the
170 probe remained inside the cell for 3 min ± 10 s. After this period, the probe was retracted, and the lifetime
171 values of the cell were captured again. Next, we compared responses under mechano-chemically
172 challenging conditions: injection of CytoD (Fig. 2C) or DMSO (*SI Appendix*, Fig. S3). A markedly higher
173 tension at the indentation site was observed for cylindrical probes compared to pyramidal ones. As
174 observed before (Fig. 1D), cylindrical probes exert a higher tension at the indentation site both with and
175 without CytoD injection. In the case of pyramidal probes, tension increased at the indentation site at "mech"
176 state but remained constant for the entire "mech + inj" state. In contrast, by cylindrical probes tension
177 increases at the indentation site during the "mech" state and increases with time after injection of CytoD
178 ("mech + inj"). After removal of the stimulus, tension at the indentation site shows an increase for pyramidal
179 probes and a slight decrease for cylindrical probes, consistent with the results shown in Fig 1D.

180 Time-lapse lifetime images of representative cells were recorded at various stages: before, during
181 mechanical stimulus ("mech"), after mechanical stimulus and injection ("mech + inj"), and post-retraction,
182 using pyramidal and cylindrical probes (Fig. 2D). Lifetime changes were calculated by subtracting each
183 cell's initial lifetime value and averaging these changes for each condition (CytoD or Cont), both during (Fig.
184 2E) and after the stimulus (Fig. 2F). CytoD-injected and control cells showed a similar tension across all
185 the ROIs in the case of pyramidal probes (Fig. 2E, top row). For cylindrical probes, CytoD-injected cells
186 exhibited a slight increase (p-value of 0.087) at the ER and a significant increase (p-value of 0.015) at the
187 NE when compared to control cells (Fig. 2E, bottom row). Interestingly, after retracting probes (Fig. 2F),
188 tension at the ER and the NE remained higher for CytoD-treated cells compared to control groups when
189 challenged by cylindrical probes. By retracting pyramidal probes, similar levels of tension were observed

190 for CytoD- and control groups within all the ROIs. In agreement with Fig. 1D, retracting pyramidal probes
191 imposed an additional mechanical stress onto the cell (Fig 2 E and F).

192 Elevated tension at the NE and indentation site is likely linked to actin filaments loss in CytoD-injected cells,
193 as actin filaments known to protect nuclei from the excessive mechanical stress.[36] Reportedly, external
194 mechanical stimulation of cells as well as intensive stretching of the NE during cell migration trigger a
195 transient formation of an actin rim around the nucleus or actin cap which is hypothesized to protects nuclear
196 content from mechanical damage by minimizing the nuclear deformation.[37] Therefore, hindering actin
197 polymerization by CytoD injection inhibits actin cap formation which otherwise dissipates the excessive
198 strain thus lowering the tension as a response to the external stimuli (Fig. 2G).

199 Furthermore, the ER displayed an increasing tension with time. As the NE is contiguous with the ER,
200 stretching and deforming the nucleus is likely to increase the membrane tension in the neighboring ER[38].
201 Additionally, the ER extends throughout the entire cell. Therefore, when targeting the nucleus even with
202 sharpened cylindrical probes, the ER is likely affected as well. However, similar tension at the ER and NE
203 for CytoD-injected and control cells during and after stimuli were observed when pyramidal probes were
204 used (Fig. 2F). The pyramidal probes with a bigger apex size compared to cylindrical ones insert a
205 mechanical disturbance directly to the ER and the NE while targeting the nucleus. This results in similarly
206 elevated tensions for both control and CytoD-injected cells when stimulated with pyramidal probes.

207 Additionally, the interplay between actin dynamics and mechanotransmission at the ER and NE highlights
208 the complexity of cellular mechanoresponses and emphasizes the need for further investigation into their
209 cross-reactivity and directionality. Thus, we applied mechano-chemical triggering to a variety of target
210 organelles, including the peripheral ER, nucleus, and cell periphery and further studied the tension
211 propagation *in situ* as a response to these stimuli.

212 Interconnected mechano-crosstalk between ER, nucleus, and actinomyosin: investigating the 213 impact of target organelle for the mechano-chemical stimuli.

214 The mechanical crosstalk between the ER, nucleus, and cytoskeleton is complex because of their intricate
215 interconnection.[39] While it is acknowledged that the nucleus serves as an endpoint for the dispersion of
216 forces, there is limited research specifically addressing cross-reactivity and directionality of mechano-
217 signaling between these subcellular components. Therefore, a cylindrical probe was used for indentation
218 on either the peripheral ER, the nucleus (with minimal ER lumens above) or the cell periphery with limited
219 ER involvement (Fig. 3 A and B). Besides, intracellular injection of either CytoD or DMSO (control) was
220 performed. In parallel, the tension at the ER and the NE of cells was monitored during (Fig. 3C) and after
221 (Fig. 3D) mechano-chemical triggering. When the nucleus was targeted (Fig. 3C, top row), CytoD-injected
222 cells showed higher tension at both the ER and NE compared to the control group. Conversely, for cell
223 periphery-targeted cells (Fig. 3C, bottom row), control cells showed a higher tension at both the ER and NE
224 compared to CytoD-injected cells. Interestingly, when the ER was subjected to the same stimuli (Fig. 3C,

225 middle row), no detectable change was observed between the cells injected with or without CytoD.
226 Following the probe retraction, tension at the ER and NE was higher for CytoD-injected compared to control
227 cells when the ER and nucleus were targeted (Fig. 3D). In contrast, in cells targeted for the cell periphery,
228 slightly lower tension at the ER and similar tension at the NE were observed for CytoD-treated compared
229 to control cells.

230 Higher tension at the ER for control cells compared to CytoD-injected cells suggests actin networks transmit
231 strain and tension intracellularly, unlike intermediate filaments which absorb mechanical stress, preventing
232 it from reaching the nucleus.[40] Therefore, interrupting actin filaments likely keep tension localized at the
233 indentation site. This is validated by higher tension transfer to the ER in control cells compared to CytoD-
234 treated ones when the cell periphery is targeted (Fig. 3C, top and bottom rows). The ER's complex
235 morphology consists of many curved structures of lumens and disks which can deform when subjected to
236 external mechanical perturbation, making it prone to absorb stress and strain when directly targeted. That
237 could explain the similar tension levels in both CytoD-injected and control cells during ER indentation.
238 Notably, unlike nucleus-targeted cells, ER-targeted cells only show increased tension at the ER and NE in
239 CytoD-injected cells compared to control ones after stimulation. This suggests fundamental differences in
240 the mechanical coupling of the nucleus and the ER to the cytoskeleton. While the nucleus maintains direct,
241 structural actin connections through the nuclear lamina and LINC complexes[41], making it immediately
242 sensitive to actin disruption, the ER relies on indirect, signaling-mediated cytoskeletal interactions[42,43].
243 Thus, the ER functions as a dynamic tension buffer that engages cytoskeletal support primarily during active
244 repair processes following mechanical perturbation. This explains why nuclear probing reveals immediate
245 tension differences in actin-disrupted cells, while ER probing only shows post-retraction effects.
246 Consequently, statistical analysis detects significant differences between test and control groups after
247 probe removal, but not during probe contact in ER-targeted experiments. Yet, when the nucleus is targeted,
248 higher tension at both the NE and the ER is recorded for CytoD-treated compared to control cells both
249 during and after the stimuli. Such distinct mechanoresponse patterns from the ER and the NE (Fig. 3C, top
250 and middle rows) also hint at a directional mechano-crosstalk between the ER and the nucleus of a
251 stimulated cell.

252 Nuclear lamins regulate nuclear mechanoresponse. Therefore, we investigated how different lamins impact
253 mechano-signaling in HeLa cells upon mechano-chemical stimulation of the nucleus, to shed light on
254 dynamic tension responses.

255 Lamin A/C's autonomous contribution to nucleus mechanoresponsiveness and its dependence on 256 B-type lamins only beyond a sustained force threshold.

257 The nuclear lamina regulates nuclear tension and contributes to cellular mechanotransmission.[44] Lamin
258 A/C modulates nuclear stiffness and chromatin remodeling,[11] while its spatial distribution determines
259 nuclear deformability.[45] B-type lamins have little effect on nuclear stiffness[45] but maintain NE integrity.[46]
260 Moreover, a balance between lamin A/C and lamins B1 and B2 is important for nuclear elasticity, with an

261 increased ratio of lamin A/C to the B-type lamins corresponding to a stiffer nucleus. The interplay between
262 A- and B-type lamins, their post-translational modifications, and their impact on governing the nuclear
263 deformability thus genome organization remain underexplored.[47] Here, we examined the contribution of
264 nuclear lamins to changes in membrane tension using HeLa cells with altered nuclear lamina composition
265 upon downregulation of A-type and/or B-type lamins.

266 Firstly, WT and *LMNA* KO HeLa cells were subjected to RNA interference (RNAi), using a non-targeting
267 silencing RNA (siRNA) control pool (siCtrl) or pools of siRNAs targeting lamin B1 and lamin B2 (siLMNB)
268 for simultaneous KD of both B-type lamins. The use of RNAi yielded 4 groups of conditions: WT-siCtrl (WT),
269 *LMNA* KO-siCtrl (A-KO), WT-siLMNB (B-KD) and *LMNA* KO-siLMNB (A-KO/B-KD). Western blot analysis
270 confirmed successful depletion of corresponding lamins in each group (*SI Appendix*, Fig. S4). Cells were
271 then stained with the ER Flipper TR dye and assessed for changes in tension levels (Fig. 4A). Lifetime
272 values at the ER and NE were quantified and compared for the different groups (WT, A-KO, B-KD and A-
273 KO/B-KD; Fig. 4B). Higher tension was captured at the ER and NE for both A-KO and B-KD compared to
274 WT cells. A-KO cells displayed significantly higher tension at the ER compared to WT cells, whereas B-KD
275 cells showed a slightly elevated tension level in comparison to WT. Surprisingly, the A-KO/B-KD group
276 showed no captured changes in tension at either the ER or NE in comparison to WT cells. Next, we indented
277 cells by cylindrical probes followed by CytoD injection (Fig. 4C), and quantified tension level in the same
278 manner as before (Fig. 4 D). A significantly lower tension at the ER, NE and indentation site for A-KO
279 compared to WT cells were detected. Intriguingly for B-KD cells, similar tension levels were observed at
280 both the NE and the indentation site when compared to WT cells. At the ER though, like A-KO cells, B-KD
281 cells showed lower tension in response to external stimulus when compared to WT cells. Surprisingly, no
282 changes in tension level of A-KO/B-KD cells were detected compared to WT cells. As varying lamin
283 compositions may alter nuclear stiffness, we also measured indentation depth under a constant 150 nN
284 force (SI Appendix, Fig. S6). We found no statistically significant difference in the indentation depth between
285 groups. The differing tension responses are therefore due to intrinsic differences in molecular mechanics
286 under identical stimulus. Examining the kinetic traits of WT and A-KO/B-KD cells revealed a reduced slope
287 in the tension response from cells lacking A-type and B-type lamins, particularly noticeable in the steady-
288 state response at 4 min post-stimulus (*SI Appendix*, Fig. S7).

289 These results align with earlier findings stating that cells lacking lamin A/C, but not Lamin B1 and B2, have
290 softer nuclei with a more deformable NE, thus dissipating the stress and lowering the tension at the NE[48,49]
291 This leads to a lower tension level at the NE for A-KO cells compared to WT cells when exposed to external
292 stimuli. The elevated wrinkles in the NE of lamin A/C KO cells[50] might play a role in dissipating stress and
293 reducing tension during mechanical stimuli, particularly when these wrinkles open due to the deformation.
294 In essence, a nucleus without A-type lamins appears less mechanoresponsive, as it likely absorbs forces
295 through bending rather than transferring them. In agreement with the previous studies, B-type lamins on
296 the other hand, do not affect nuclear stiffness, and deformation, thus its tension response.

297 Lower tension in A-KO and B-KD cells compared to WT cells suggests that both A-type and B-type lamins
298 influence the tension crosstalk from the NE to the ER. Examining their tension response reveals that when
299 actin filaments are disturbed, lamin A/C primarily affects the immediate response of nucleus to physical
300 deformation of the nucleus. Conversely, B-type lamins become more significant under sustained load. In
301 other words, lamin A/C alone can contribute to the nucleus's mechanoresponsive abilities, but *LMNA* KO
302 cells become less mechanoresponsive than WT cells and depend on the supportive function of B-type
303 lamins. This implies that even at this juncture, A-KO/B-KD cells under prolonged stress might show reduced
304 mechanoresponses compared to WT cells, notably with a decrease in tension at the indentation site
305 recorded after 3 minutes post-stimulus (Fig. 4D).

306 The nucleus stretches rapidly in response to a step-function load and undergoes a viscoelastic transition
307 with sustained load, taking seconds to reach a steady state. This behavior depends on lamina composition
308 and chromatin states,[51] possibly aiming to dissipate mechanical energy and prevent nuclear damage. We
309 discerned the different roles of lamin A/C versus lamin B1 and B2 in the viscoelastic response of the nucleus
310 and the ER. This process separated the immediate response ("elastic"), due to the probe indentation
311 measured at "mech" state from a gradual deformation ("creep") under constant force applied during "mech
312 + inj" state. Creep response reflects cell's viscous property, with higher creep reflecting lower cell's
313 viscosity. The viscoelastic response was influenced by CytoD injection as a chemical stimulus, followed by
314 a continuous load of 150 nN for 4 min ± 10 s. The results are depicted as accumulated bar plots in the top
315 panel of Fig. 4E. At the ER, similar levels of elastic and viscous responses were detected for cells with
316 different lamin proteins levels compared to WT cells. At the NE, though, lower elasticity in *LMNA* KO cells
317 and similar viscous response in all the cells were captured. At indentation site, cells lacking A-type lamins
318 show a reduced elastic property while cells with deficiencies in B-type-lamins have lower creep and thus
319 higher viscous response. Further the temporal relaxation of tension at the ER, NE and indentation site were
320 investigated both immediately after the stimulus (Fig. 4E, bottom row) and 5 min post-stimulus (*SI Appendix*,
321 Fig. S8). Relaxation property was quantified by comparing the lifetime value after probe retraction to the
322 last time point of stimuli at "mech + inj" state. A higher relaxation value indicates greater recovery of the
323 deformed structure and thus a stronger elastic component of the mechanoresponse. Following the stimulus,
324 cells deficient in both A-type and B-type lamins displayed increased relaxation at the indentation site which
325 experiences maximum deformation (Fig. 4E, bottom right). Finally, 5 min post-stimulus, cells with diverse
326 depletion of lamins exhibit a consistent relaxation extent across various ROIs (*SI Appendix*, Fig. S8). These
327 findings suggest A-type lamins contribute to nuclear elasticity, while B-type lamins influence viscous
328 behavior during sustained deformation and disrupted actin polymerization (Fig. 4E, top right). Nonetheless,
329 previously a potential role for lamin A in viscous response of NE in both intact tissue and suspended cells
330 has been reported.[52,53] In our study, the disruption of the dynamic actin network by CytoD injection suggests
331 that the interaction between lamin A/C and the actin meshwork may be essential for maintaining the viscous
332 properties of lamin A. Higher relaxation in A-KO/B-KO cells immediately upon removal of probes, reflecting
333 higher tension restoration, may be linked to the absence of actin filaments alongside the lamins depletion.

334 In contrast, WT cells and cells lacking either A-type- or B-type-lamins maintain tension, releasing it gradually
335 over time. Similar relaxation values for all cells at 5 min post-stimulus indicate cytoskeletal reorganization
336 and NE adaptations, allowing stress recovery independently of nuclear lamina. Since nuclear lamina
337 organization affects how cells detect and respond to mechanical stimuli, we aimed to dissect the roles of
338 cytoskeletal components in initiating the mechanoresponse of the nucleus and ER after mechanical and
339 chemical stimuli with various molecular disruptors (CytoD, Noco, and their combination).

340 **Modulating mechanoresponse: impact of lamin A/C on microtubule dynamics and adaptive**
341 **mechanosensitivity.**

342 The nuclear lamina contributes to organize the cytoskeleton[40], with other components like actin filaments
343 and microtubules enabling cells to sense and respond to mechanical stimuli (Fig. 2G).[54] In particular, loss
344 of lamin A/C is linked to decreased myosin II contractility and in some cases to the absence of apical stress
345 fibers,[55] which disrupts cytoskeletal dynamics and affects how cells interpret mechanical signals.
346 Conversely, MT depolymerization can enhance actomyosin contractility via the RhoA-Rock pathway,
347 altering cell mechanics and nuclear properties. Considering the intricate interplay between the cytoskeleton,
348 nucleus, and mechanical cues in cellular behavior, we assessed how changes in cytoskeletal components
349 and lamin A/C affect cellular mechanoresponse and disease contribution.

350 Noco- and CytoD-Noco-treated WT cells had low tension across ROIs. A-KO cells showed higher tension
351 at the ER and NE with Noco or CytoD-Noco compared to CytoD alone. No difference in tension between
352 Noco and CytoD-Noco groups at the ER and NE.

353 Actomyosin and microtubules, due to their dynamic response compared to intermediate filaments[56], were
354 studied for their roles in initiating nuclear mechanoresponse. We targeted the cytoskeleton of WT and A-
355 KO cells with different disruptors including CytoD, Nocodazole (Noco, a microtubule inhibitor), and their
356 combination (CytoD-Noco), each at 50 μM, resulting in 0.5 μM upon intracellular injection. Noco binds to β-
357 tubulin subunits, thereby inhibiting the polymerization of tubulins into MTs.[57] These investigations focused
358 on WT and lamin A/C deficient cells, due to lamin A/C's distinctive roles in NE mechanoresponse as
359 examined in section 2.4. Tension response to stimuli were quantified at various ROIs (Fig. 5 A and B).
360 Notably, WT cells mechanoresponse is governed by MTs presence, showing increased tension in CytoD-
361 treated cells compared to Noco- or CytoD-Noco-treated cells at the ER, NE, and the indentation site.
362 Tension in WT cells with MTs (CytoD-treated cells) compared to those with less MTs (either Noco- or CytoD-
363 Noco-treated cells) significantly increased upon stimulation. Noco- and CytoD-Noco-treated WT cells
364 exhibited similarly low levels of tension across all ROIs. Cells lacking lamin A/C showed distinct responses
365 to the aforementioned drugs compared to WT cells. *LMNA* KO cells displayed higher tension at the ER and
366 NE when subjected to Noco or CytoD-Noco (less MTs in function) compared to when exposed to CytoD
367 alone. Interestingly, at the ER and NE there were no difference in tension values between Noco and CytoD-
368 Noco groups. At the indentation site, A-KO cells showed similar trends in the ER and NE for CytoD and
369 Noco treated cells. Interestingly, A-KO cells lacking both actin filaments and MTs had the lowest tension.

370 Higher tension in WT cells with active MTs compared to those with less MTs (Noco- and CytoD-Noco-
371 treated) indicates MTs' dominant role in tension propagation within the ER-NE network. This is likely due
372 to their close association with the ER network. Microtubules seemingly maintain tension within the ER-NE
373 network rather than transferring it, independently of actin filaments (Fig. 5B, top row). Yet, actin filaments
374 lower the tension in cells with intact MTs (Fig. 2 E and F). In A-KO cells, MTs facilitate nuclear deformation.[58]
375 Thus, in A-KO cells, Noco and CytoD-Noco treatment minimizes the deformation of nucleus and increases
376 tension at the ER and NE. On the other hand, CytoD treated A-KO cells with functional MTs exhibit higher
377 deformation and thus lower tension. Similar tension levels in Noco- and CytoD-Noco-treated A-KO cells at
378 the ER and NE indicate actin filaments independence. Lamin A/C forms the perinuclear actin cap[50,59],
379 explaining high tension at the indentation site in Noco-treated A-KO cells compared to WT cells despite
380 having active actin filaments. Low tension in CytoD-Noco-injected A-KO cells suggests a highly deformable
381 nuclear membrane, despite lacking active microtubules at the indentation site.

382 Next, elastic and viscous (derived from creep behavior) components of tension response in WT and A-KO
383 cells under various drug treatments were quantified (*SI Appendix*, Fig. S9A). WT cells showed decreased
384 creep (increased viscous response) of WT cells with CytoD-Noco compared to CytoD treatment, but no
385 significant difference between CytoD-Noco and Noco treatment across all ROIs. In contrast, A-KO cells had
386 the lowest creep (highest viscous response) in the ER with CytoD treatment. In other words, under lamin
387 A/C deficiency, microtubules reduce tension and diminish the creep response.

388 Finally, temporal tension relaxation was studied upon probe removal and diminishing the mechanical
389 stimulus. Relaxation was quantified as a change in lifetime immediately after probe retraction (*SI Appendix*,
390 Fig. S9) and 5 min (Fig. 5C) post-stimulus, both with respect to the last time point during stimuli. WT and
391 lamin A/C deficient cells exhibited similar tension immediately after probe retraction, regardless of the
392 injected drug. Additionally, lamin A/C deficient cells treated with various drugs had consistent relaxation
393 compared to WT across all ROIs. Though, relaxation at 5 min post-stimulus depended on drug treatment,
394 especially at the ER and NE. WT cells treatment with CytoD or Noco alone had higher relaxation compared
395 to CytoD-Noco at the ER. Instead, A-KO cells showed the lowest relaxation with CytoD and highest with
396 CytoD-Noco treatment, 5 min post stimulus at the ER and NE. Notably, no significant differences in
397 relaxation were found among drug treatments at the indentation site for both WT and *LMNA* KO cells.

398 Collectively, both actin and microtubules contribute to the cell's elastic mechanoresponse, as shown by the
399 similar elastic relaxation in WT cells treated with CytoD or Noco. Interestingly, loss of both A-type and B-
400 type lamins does not affect tension at the NE or ER, unlike the individual loss of either lamin type. This
401 highlights the complex interplay between different lamins and cytoskeletal elements in cellular mechanics.
402 Microtubules play a lesser role in conferring viscous properties (time-dependent) to healthy cells, indicated
403 by lower creep and higher viscous response of the ER when exposed to microtubule-disturbing drugs (Noco
404 or CytoD-Noco). This is due to the rapid dynamics of microtubules with critical roles in cell division and
405 intracellular transport.[60,61] In lamin A/C-deficient cells, MTs contribute to a more viscous mechanoresponse,

406 shown by higher creep and lower viscous response with microtubule-disturbing drugs (Noco or CytoD-
407 Noco). This adaptation in microtubule mechanosensitivity may be due to the absence of the actin cap in
408 lamin A/C-depleted cells.

409 Conclusion

410 Combining FluidFM with FLIM enabled real-time, high-resolution mapping of intracellular tension dynamics
411 upon quantitative injection of active components while maintaining a constant mechanical stimulus. The
412 proposed approach allowed investigation of intracellular mechanotransmission crucial for
413 mechanotransduction regulation and cell fate control. CytoD Injection, as *in situ* mechano-chemical trigger,
414 disrupted actin filament dynamics, altering tension at the ER and NE. Sharpened cylindrical probes
415 increased tension locally on the nucleus, and CytoD-injection increased tension at the ER and NE
416 compared to control injection. Pyramidal probes required a higher force to puncture the nuclear membrane
417 (50 nM) compared to that of the cylindrical one (10 nN). Membrane puncture resulted in tension relaxation
418 at the NE. Increased indentation force for sealed injection showed lower tension at the NE and the ER with
419 cylindrical probes compared to pyramidal ones. Changing the incident site from the nucleus to the ER and
420 cell periphery confirmed that actin filaments alone transmit tension away from the deformation site. In
421 contrast, CytoD injection and actin filament disturbance retained tension at the site of incidence. Direct ER
422 targeting suppressed tension from reaching the nucleus. This indicates specialized tension distribution
423 within cells. Nuclear lamins showed distinct responses to mechanical cues, with A-type and B-type lamins
424 affecting elastic and viscous properties, respectively. Interestingly, combined loss of lamins A and B did not
425 affect tension at the NE or ER, suggesting a compensatory mechanism needing further investigation.

426 In conclusion, our study examined how the cytoskeleton, particularly actin and microtubules, collaborates
427 with nuclear lamina to initiate nuclear mechanoresponse. In WT cells MTs maintained tension, while actin
428 filaments lowered it in responding to external stress. In lamin A/C-deficient cells, microtubules facilitated
429 nuclear deformation and lowered the tension, in contrast to actin filaments. This highlights lamin A/C's role
430 in regulating the collaboration between the NE and the cytoskeleton, affecting nuclear and the ER
431 mechanoresponse. Additionally, nuclear deformation under external stimulus involves interactions between
432 chromatin and cytoskeletal components through the lamina and LINC complexes. However, the exact
433 mechanisms of chromatin involvement require further study. Lastly, the intermediate filament system,
434 particularly vimentin, also plays a key role in nuclear integrity and connecting to other organelles like
435 mitochondria. Future studies should explore their contributions to mechanotransmission phenomena.

436 Methods

437 For detailed procedures of the following steps, see *SI Appendix*.

438 **Cells Preparation.** HeLa cells with WT condition or with altered levels of lamin proteins were cultured using
439 standard procedure for adherent cells. Cells were seeded on glass bottom dishes 1 or 2 days before the

440 experiments. Just before the experiments, cells medium was changed to CO_2 independent medium and
441 cells were stained with 1 μM ER Flipper-TR, designed to report changes in membrane tension at the ER.
442 However, ER Flipper-TR dye apparently stains other endomembrane structures in addition to ER as well.

443 **FluidFM Probe Preparation.** The custom-fabricated cylindrical probes (SmartTip BV in Enschede, the
444 Netherlands) featured a tube length of 10 μm, an aperture diameter of 1 μm, and a microchannel thickness
445 of 1.5 μm.[62] Subsequently, they underwent milling with an FIB machine mounted on a SEM (Helios 5 UX,
446 ScopeM, ETH Zurich, Switzerland) to achieve sharpness at their apex (50° angle, Fig. 1 B). Both
447 customized cylindrical and purchased pyramidal probes (Cytosurge AG, Switzerland) were subjected to
448 coating with Sigmacote vapor to minimize contamination during experiments. This coating imparted anti-
449 fouling properties. The probes were baked at 100°C for 2 hours to ensure stability. Finally, the probes, filled
450 with 0.1 $mg \cdot mL^{-1}$ coumarin 120 (blue dye) plus the drug of interest (50 μM CytoD, 50 μM Noco, or 50 μM
451 CytoD + 50 μM Noco) in HEPES2 buffer, were used for intracellular injection experiments upon calibration.

452 **FluidFM-FLIM Setup.** We combined FluidFM system (FlexAFM-near-infrared scan head with a C3000
453 controller driven by the EasyScan2 software, Nanosurf AG, Switzerland) with FLIM imaging on a Leica SP8
454 FALCON inverted confocal microscope.[31] To achieve this, we removed the condenser lens and z-galvo
455 stage. The FluidFM probe was independently positioned using an elevated AFM scan head attached to a
456 custom mount. Adjustments were made to reach the substrate surface, and FLIM imaging utilized laser
457 pulses at 488 nm operating at a frequency of 40 MHz. The entire setup was maintained at a temperature
458 of 37°C. The AFM piezo movement, deflection of the cantilever, and fluidic pressure (in the case of injection
459 in mechano-chemical stimulation) were recorded utilizing a data acquisition box and a LabView script.

460 **Mechanical and Mechano-chemical Stimulation.** For the FluidFM stimuli, the probes were first calibrated
461 for spring constant and sensitivity, then approached on the HeLa cells stained with the ER-Flipper-TR dye.
462 The setpoint for the indentation force varied between 2 and 100 nN for mechanical stimulation, while it was
463 adjusted to 150 nN for the mechano-chemical stimulation assuring a successful injection. Both stimuli were
464 operated at an approach speed of 1 $\mu m.s^{-1}$, which was chosen to mimic the natural mechanical environment
465 that cells experience in the body. For mechano-chemical stimulus employing an injection pulse (100 mbar
466 for 10 s) after reaching the setpoint, probes were previously filled with the desired chemical solution.
467 Lifetime images of the target cells were concurrently captured, featuring a pixel size of 90 nm. For
468 comparison, lifetime images were collected before the stimulus, during the pause time of the mechanical
469 stimulus before injection pulse ("mech"), series of images after the injection pulse ("mech + inj") and one
470 image after retracting the probe. For experiments addressing the relaxation behavior, an additional lifetime
471 image was captured 5 minutes post-stimulus.

472 **Statistical Analysis.** Data were tested for normal distribution using the Shapiro-Wilk test before applying
473 parametric statistical methods. Differences between two groups were assessed using an unpaired two-
474 tailed Student's t-test. Where multiple comparisons were conducted, a t-test with Holm correction was
475 applied to control the false discovery rates, as indicated in the relevant sections. P-values were calculated

476 and reported for all analyses, with a significance threshold set at $p < 0.05$. The sample size for each
477 experiment (n) is provided in the figure legends, and the number of independent biological replicates (N) is
478 explicitly reported to ensure reproducibility. All statistical analyses were performed custom Python scripts.

479 **Acknowledgments.** The authors thank János Vörös and all the LBB team for insightful discussions, Edin
480 Sarajlic (Smartip BV, NL) for fabrication of customized FluidFM probes, Stephen Wheeler for his workshop
481 support, Joakim Reuteler and Justine Kusch at ScopeM facility (ETH Zurich) for microscopy support, and
482 Aldo Riccardo at cleanroom facility (D-ITET ETH Zurich). E.Z.E. and I.L. received support from the EUREKA
483 Network (Eurostars Project E!11644 "SOUL" to T.Z.). Additionally, E.Z.E. acknowledge funding from the
484 Swiss National Science Foundation (Sinergia Grant CRSII5_202301 to T.Z.). U.K. acknowledges support
485 by the Swiss National Science Foundation (project grant 310030_219203 and SNSF Advanced Grant
486 TMAG-3_209245).

487 **Data Availability.** The datasets generated and analyzed during the current study, including the FLIM image
488 data and the Python scripts developed for the quantification of values, statistical analysis, and data
489 visualization are available in the ETH Zürich Research Collection at https://doi.org/10.3929/ethz-c-
490 000790250. Additionally, the force and pressure measurements, are available upon request.

491

492

493 **References**

494 1 Faria, M. Aggregating, polarizing, networking - The evolution of cell adhesion codes. *Biosystems*
495 **164**, 60-67 (2018).

496 2 Jonas, O. & Duschl, C. Force propagation and force generation in cells. *Cytoskeleton (Hoboken)*
497 **67**, 555-563 (2010).

498 3 Li, Y., Wong, I. Y. & Guo, M. Reciprocity of Cell Mechanics with Extracellular Stimuli: Emerging
499 Opportunities for Translational Medicine. *Small* **18 (36)**, 2107305-2107705 (2022).

500 4 Swaminathan, V. & Gloerich, M. Decoding mechanical cues by molecular mechanotransduction.
501 *Curr Opin Cell Biol* **72**, 72-80 (2021).

502 5 Mathieu, S. & Manneville, J. B. Intracellular mechanics: connecting rheology and
503 mechanotransduction. *Curr Opin Cell Biol* **56**, 34-44 (2019).

504 6 Lityagina, O. & Dobreva, G. The LINC Between Mechanical Forces and Chromatin. *Front Physiol*
505 **12**, 710809 (2021).

506 7 Kirby, T. J. & Lammerding, J. Emerging views of the nucleus as a cellular mechanosensor. *Nat Cell*
507 *Biol* **20**, 373-381 (2018).

508 8 Kim, T. J. *et al.* Distinct mechanisms regulating mechanical force-induced Ca^{2+} signals at the
509 plasma membrane and the ER in human MSCs. *Elife* **4**, e04876 (2015).

510 9 Mahecic, D. *et al.* Mitochondrial membrane tension governs fission. *Cell Rep* **35**, 108947 (2021).

511 10 Guet, D. *et al.* Mechanical role of actin dynamics in the rheology of the Golgi complex and in Golgi-
512 associated trafficking events. *Curr Biol* **24**, 1700-1711 (2014).

11 Donnaloja, F., Carnevali, F., Jacchetti, E. & Raimondi, M. Lamin A/C Mechanotransduction in Laminopathies. *Cells* **9**, 1306 (2020).

12 Zheng, M., Jin, G. & Zhou, Z. Post-Translational Modification of Lamins: Mechanisms and Functions. *Frontiers in Cell and Developmental Biology* **10**, 864191 (2022).

13 Wintner, O. *et al.* A Unified Linear Viscoelastic Model of the Cell Nucleus Defines the Mechanical Contributions of Lamins and Chromatin. *Advanced Science* **7**, 1901222 (2020).

14 Patil, S. & Sengupta, K. Role of A- and B-type lamins in nuclear structure-function relationships. *Biology of the Cell* **113**, 295-310 (2021).

15 Dalton, C. J. & Lemmon, C. A. Fibronectin: Molecular Structure, Fibrillar Structure and Mechanochemical Signaling. *Cells* **10**, 2443 (2021).

16 Hang, X. *et al.* Nanosensors for single cell mechanical interrogation. *Biosens Bioelectron* **179**, 113086 (2021).

17 Broussard, J. A. *et al.* The desmoplakin-intermediate filament linkage regulates cell mechanics. *Mol Biol Cell* **28**, 3156-3164 (2017).

18 Blakely, B. L. *et al.* A DNA-based molecular probe for optically reporting cellular traction forces. *Nat Methods* **11**, 1229-1232 (2014).

19 Tian, Q., Keshri, P. & You, M. Recent developments in DNA-based mechanical nanodevices. *Chem Commun (Camb)* **58**, 4700-4710 (2022).

20 Català-Castro, F. *et al.* Measuring age-dependent viscoelasticity of organelles, cells and organisms with time-shared optical tweezer microrheology. *Nature Nanotechnology* **20**, 411-420 (2025).

21 Li, K. & Jan, Y. N. Experimental tools and emerging principles of organellar mechanotransduction. *Trends in Cell Biology* (2025).

22 Freikamp, A., Cost, A. L. & Grashoff, C. The Piconewton Force Awakens: Quantifying Mechanics in Cells. *Trends Cell Biol* **26**, 838-847 (2016).

23 Eder, D., Basler, K. & Aegerter, C. M. Challenging FRET-based E-Cadherin force measurements in Drosophila. *Sci Rep* **7**, 13692 (2017).

24 Goujon, A. *et al.* Mechanosensitive Fluorescent Probes to Image Membrane Tension in Mitochondria, Endoplasmic Reticulum, and Lysosomes. *J Am Chem Soc* **141**, 3380-3384 (2019).

25 Colom, A. *et al.* A fluorescent membrane tension probe. *Nat Chem* **10**, 1118-1125 (2018).

26 Meister, A. *et al.* FluidFM: Combining Atomic Force Microscopy and Nanofluidics in a Universal Liquid Delivery System for Single Cell Applications and Beyond. *Nano Letters* **9**, 2501-2507 (2009).

27 Guillaume-Gentil, O. *et al.* Tunable Single-Cell Extraction for Molecular Analyses. *Cell* **166**, 506-516 (2016).

28 Guillaume-Gentil, O. *et al.* Force-Controlled Fluidic Injection into Single Cell Nuclei. *Small* **9**, 1904-1907 (2013).

29 Guillaume-Gentil, O. *et al.* Single-Cell Mass Spectrometry of Metabolites Extracted from Live Cells by Fluidic Force Microscopy. *Analytical Chemistry* **89**, 5017-5023 (2017).

30 Li, M., Liu, L & Zambelli, T. FluidFM for single-cell biophysics. *Nano Res.* **15**, 773–786 (2022).

31 Lüchtefeld, I., Pivkin, I.V., Gardini, L., Zare-Eelanjegh, E., Gäbelein, C., Ihle, S.J., Reichmuth, A.M., Capitanio, M., Martinac, B., Zambelli, T. and Vassalli, M. Dissecting cell membrane tension dynamics and its effect on Piezo1-mediated cellular mechanosensitivity using force-controlled nanopipettes. *Nature Methods* **21**, 1063-1073 (2024).

32 Yang, W., Lacroix, D., Tan, L. & Chen, J. Revealing the nanoindentation response of a single cell using a 3D structural finite element model. *Journal of Materials Research* **36**, 2591-2600 (2021).

557 33 Ulferts, S., Prajapati, B., Grosse, R. & Vartiainen, M. K. Emerging Properties and Functions of Actin
558 and Actin Filaments Inside the Nucleus. *Cold Spring Harb Perspect Biol* **13**, a040121 (2021).

559 34 Dupont, S. & Wickström, S. A. Mechanical regulation of chromatin and transcription. *Nat Rev Genet*
560 **23**, 624-643 (2022).

561 35 Gokhin, D. S., et al. Dynamic actin filaments control the mechanical behavior of the human red
562 blood cell membrane. *Molecular biology of the cell* **26**, 1699-1710 (2015).

563 36 Hoffman, L. M. *et al.* Mechanical stress triggers nuclear remodeling and the formation of
564 transmembrane actin nuclear lines with associated nuclear pore complexes. *Mol Biol Cell* **31**, 1774-
565 1787 (2020).

566 37 Fracchia, A., Asraf, T., Salmon-Divon, M. & Gerlitz, G. Increased Lamin B1 Levels Promote Cell
567 Migration by Altering Perinuclear Actin Organization. *Cells* **9**, 2161 (2020).

568 38 Enyedi, B. & Niethammer, P. Nuclear membrane stretch and its role in mechanotransduction.
569 *Nucleus* **8**, 156-161 (2017).

570 39 Pruitt, B. L., Dunn, A. R., Weis, W. I., & Nelson, W. J. Mechano-Transduction: From Molecules to
571 Tissues. *PLoS biology* **12**, e1001996 (2014).

572 40 Oses, C. *et al.* From the membrane to the nucleus: mechanical signals and transcription regulation.
573 *Biophys Rev* **15**, 671-683 (2023).

574 41 Maurer, M. & Lammerding, J. The Driving Force: Nuclear Mechanotransduction in Cellular
575 Function, Fate, and Disease. *Annu Rev Biomed Eng* **21**, 443-468 (2019).

576 42 Shi, X. *et al.* Actin nucleator formins regulate the tension-buffering function of caveolin-1. *J Mol Cell*
577 *Biol* **13**, 876-888 (2022).

578 43 van Vliet, A. R. & Agostinis, P. PERK and filamin A in actin cytoskeleton remodeling at ER-plasma
579 membrane contact sites. *Molecular & Cellular Oncology* **4**, e1340105 (2017).

580 44 Guilluy, C. *et al.* Isolated nuclei adapt to force and reveal a mechanotransduction pathway in the
581 nucleus. *Nat Cell Biol* **16**, 376-381 (2014).

582 45 Srivastava, L., Ju, Z., Ghagre, A. & Ehrlicher, A. Spatial distribution of lamin A/C determines nuclear
583 stiffness and stress-mediated deformation. *Journal of Cell Science* **134**, jcs248559 (2021).

584 46 Camps J, E. M., Ried T The role of lamin B1 for the maintenance of nuclear structure and function.
585 *Nucleus* **6(1)**, 8-14 (2015).

586 47 Cho, S. *et al.* Mechanosensing by the Lamina Protects against Nuclear Rupture, DNA Damage,
587 and Cell-Cycle Arrest. *Developmental Cell* **49**, 920-935 (2019).

588 48 Williamson, A., Zhu, Z. & Yuan, Z. Epigenetic mechanisms behind cellular sensitivity to DNA
589 damage. *Cell Stress* **2**, 176-180 (2018).

590 49 Solovei, I. *et al.* LBR and lamin A/C sequentially tether peripheral heterochromatin and inversely
591 regulate differentiation. *Cell* **152**, 584-598 (2013).

592 50 Kim, J. *et al.* Nuclear lamin A/C harnesses the perinuclear apical actin cables to protect nuclear
593 morphology. *Nature Communications* **8**, 2123 (2017).

594 51 Buxboim, A. *et al.* Scaffold, mechanics and functions of nuclear lamins. *FEBS Letters* **597**, 2791-
595 2805 (2023).

596 52 Swift, J. *et al.* Nuclear Lamin-A Scales with Tissue Stiffness and Enhances Matrix-Directed
597 Differentiation. *Science* **341**, 1240104 (2013).

598 53 Harada, T. *et al.* Nuclear lamin stiffness is a barrier to 3D migration, but softness can limit survival.
599 *Journal of Cell Biology* **204**, 669-682 (2014).

600 54 Liu, Y., Mollaeian, K., Shamim, M. & Ren, J. Effect of F-actin and Microtubules on Cellular
601 Mechanical Behavior Studied Using Atomic Force Microscope and an Image Recognition-Based
602 Cytoskeleton Quantification Approach. *International Journal of Molecular Sciences* **21**, 392 (2020).

603 55 Alisafaei, F., Jokhun, D. S., Shivashankar, G. V. & Shenoy, V. B. Regulation of nuclear architecture,
604 mechanics, and nucleocytoplasmic shuttling of epigenetic factors by cell geometric constraints.
605 *Proc Natl Acad Sci U S A* **116**, 13200-13209 (2019).

606 56 Geng, J. *et al.* Microtubule Assists Actomyosin to Regulate Cell Nuclear Mechanics and Chromatin
607 Accessibility. *Research* **6**, 0054 (2023).

608 57 Blajeski, A. L., Phan, V.A., Kottke, T.J. and Kaufmann, S.H. G_1 and G_2 cell-cycle arrest following
609 microtubule depolymerization in human breast cancer cells. *The Journal of clinical investigation*
610 **110**, 91-99 (2002).

611 58 Tariq, Z. *et al.* Lamin A and microtubules collaborate to maintain nuclear morphology. *Nucleus* **8**,
612 433-446 (2017).

613 59 Kechagia, Z. & Roca-Cusachs, P. Cytoskeletal safeguards: Protecting the nucleus from mechanical
614 perturbations. *Current Opinion in Biomedical Engineering* **28**, 100494 (2023).

615 60 Akhmanova, A. & Steinmetz, M. O. Microtubule +TIPs at a glance. *J Cell Sci* **123**, 3415-3419
616 (2010).

617 61 Schaedel, L. *et al.* Microtubules self-repair in response to mechanical stress. *Nat Mater* **14**, 1156-
618 1163 (2015).

619 62 Gäbelein, C. G. *et al.* Mitochondria transplantation between living cells. *PLoS Biol* **20**, e3001576
620 (2022).

621

622

Figures

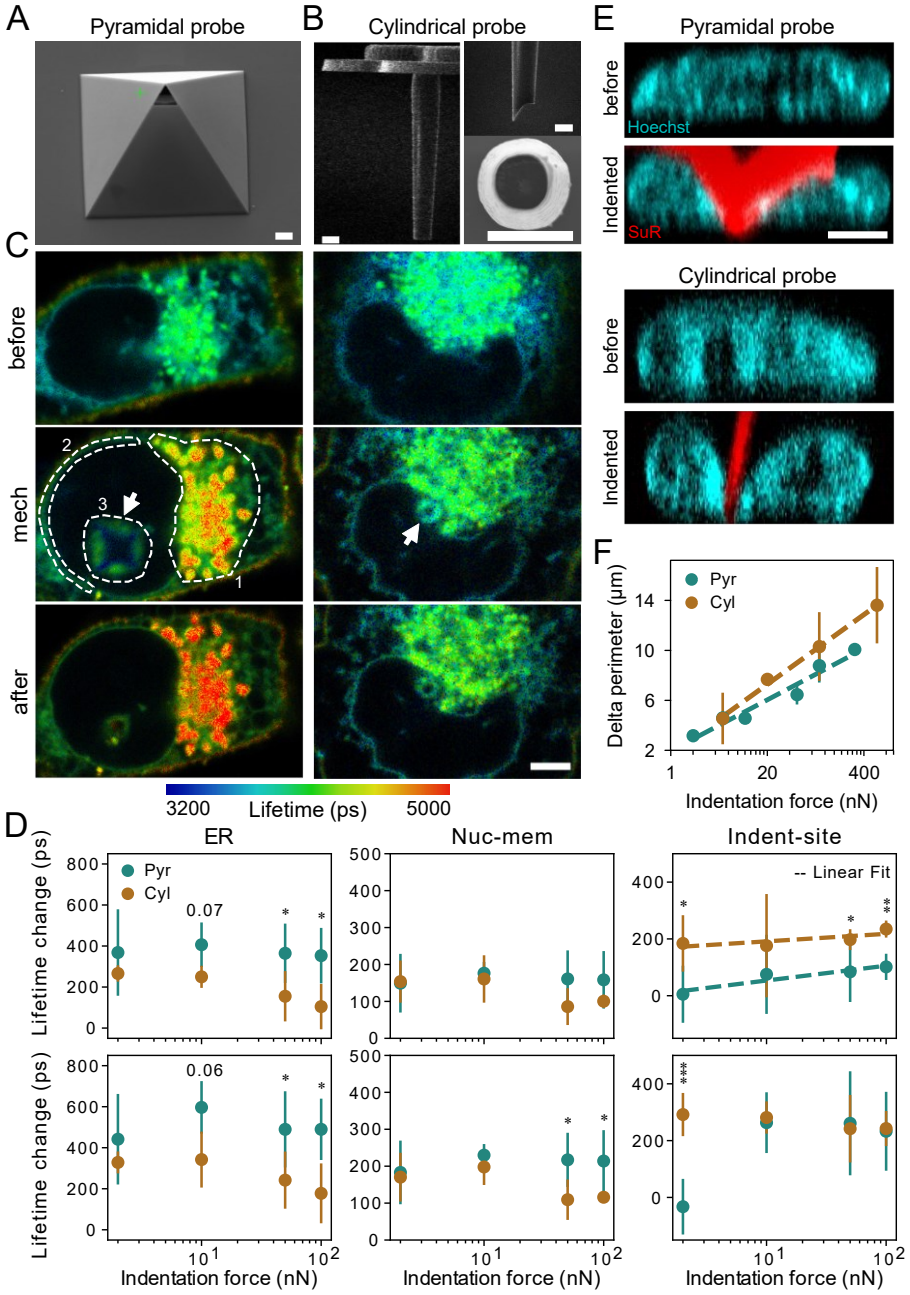

Fig. 1. FluidFM stimulation combined with FLIM readout for measuring subcellular mechanoresponse upon mechanical stimulation of nuclei.

A, B) SEM micrographs of a pyramidal probe (A) and a cylindrical probe (B) before (left) and after FIB-cut (top right). The top view of the cylinder is also shown in panel B. Scale bars represent 1 µm.

C) Lifetime images of HeLa cells stained with molecular tension probe (ER Flipper-TR) before (top), during (middle) and after (bottom) indentation at 100 nN, with pyramidal (left panel) and sharpened cylindrical probes (right panels). Arrows denote the indentation site when either pyramidal or cylindrical probes are used. Dashed lines indicate a representative selection of ROIs, encompassing 1) the ER, 2) nuclear membrane (Nuc-mem), and 3) the area around the indentation site (Indent-site). Scale bar represents 5 μm.

D) Change in lifetime during (top panel, "mech" in C) and after (bottom panel) mechanical stimulus with varied indentation forces at different ROIs: ER, nucleus membrane (Nuc-mem) and incident indentation site ("Indent-site") (Mean ± SD, $N \geq 2$, $n \geq 4$, ***$p < 0.001$, **$p < 0.01$, *$p < 0.05$, reported p-values of $0.05 \leq p < 0.1$, t-test). For mechanical stimulation, pyramidal ("Pyr") and cylindrical ("Cyl") probes with similar stiffness (2 ± 0.5 Nm-1) were utilized.

E) Lateral view of nucleus before (top panels) and during indentation (bottom panels) (indicated by "mech" in panel C) at 100 nN using pyramidal and cylindrical probes. Nuclei are stained with Hoechst dye (blue) and probes are filled with sulforhodamine dye (SuR, red). Scale bar represents 5 μm.

F) Change in perimeter of nucleus measured from confocal images at varied indentation forces, with pyramidal and sharpened cylindrical probes (Mean ± SD, $N = 2$, $n \geq 3$).

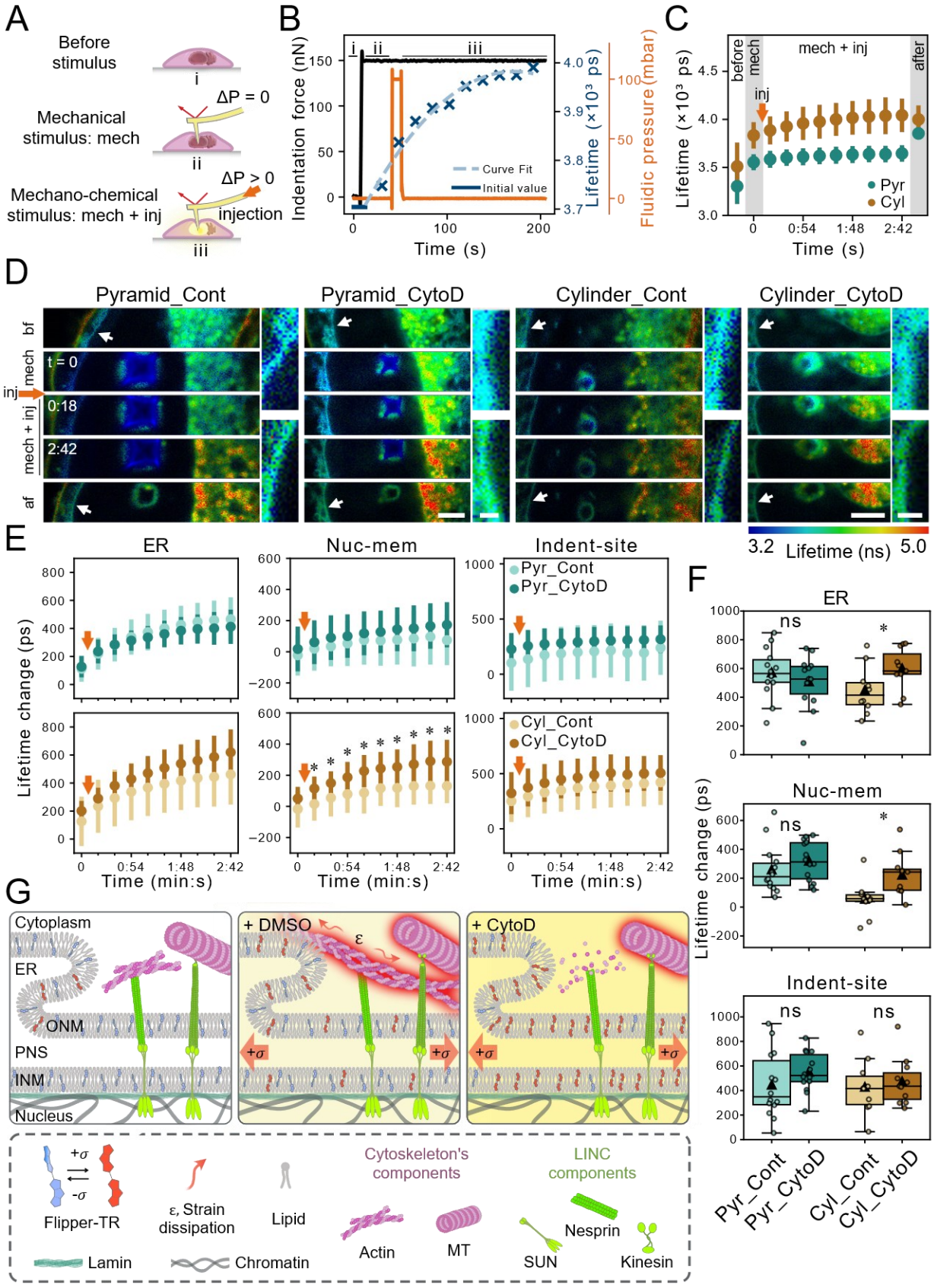
A
Before stimulus
i
Mechanical stimulus: mech
ΔP = 0
ii
Mechano-chemical stimulus: mech + inj
ΔP > 0
injection
iii
B
Indentation force (nN)
Lifetime (×10³ ps)
Fluidic pressure (mbar)
Curve Fit
Initial value
Time (s)
C
before
mech
mech + inj
after
inj
Pyr
Cyl
Time (s)
D
Pyramid_Cont
Pyramid_CytoD
Cylinder_Cont
Cylinder_CytoD
bf
mech
inj
mech + inj
af
t = 0
0:18
2:42
3.2
Lifetime (ns)
5.0
E
ER
Nuc-mem
Indent-site
Pyr_Cont
Pyr_CytoD
Cyl_Cont
Cyl_CytoD
Lifetime change (ps)
Time (min:s)
F
ER
Nuc-mem
Indent-site
ns
*
Lifetime change (ps)
Pyr_Cont
Pyr_CytoD
Cyl_Cont
Cyl_CytoD
G
Cytoplasm
ER
ONM
PNS
INM
Nucleus
+ DMSO
+ CytoD
ε
+σ
Flipper-TR
ε, Strain dissipation
Lipid
Cytoskeleton's components
LINC components
Actin
MT
Nesprin
SUN
Kinesin
Lamin
Chromatin

Fig. 2. FluidFM-FLIM mechanochemical stimulation of HeLa cell nuclei using pyramidal and cylindrical probes.

A) Schematic showing the mechanotransduction at LINC complexes before (top) and after external stimulus: mechanical (middle) or mechanochemical (bottom) stimulus. ΔP represents the fluidic pressure difference between the probe reservoir and the aperture. When this pressure difference is positive, it indicates that the injection mode of FluidFM is being utilized.

B) Concurrent readout of AFM-measured indentation force, ER Flipper-TR lifetime, and fluidic pressure pulse for injection over time. For assured injection, 150 nN was chosen as the set point for indentation using both probe geometries. Parts i, ii and iii on the graph in B and the schematic in A represent: i) before stimulus, ii) during mechanical stimulus when the probe has reached the set point on the cell without fluidic pressure application, and iii) during mechanochemical stimulus when the probe remains in contact with the cell at the set point, and a fluidic pressure pulse is applied for drug (or control) injection.

C) Absolute lifetime values before, during and after injecting HeLa cells with CytoD with pyramidal ("Pyr") and cylindrical ("Cyl") probes at indentation site (Mean ± SD, $N \geq 3$, $n \geq 11$). The orange arrow indicates the injection pulse at the specified time in the mechanochemical triggers.

D) Time-lapse lifetime images of ER Flipper-TR-stained HeLa cells before, upon indentation ("mech"), after indentation plus injection ("mech + inj") of either DMSO (as control) or 50 μM CytoD, and after retracting pyramidal (left) and cylindrical (right) probes. The numbers represent time (min:s), with time 0 corresponding to the indented state (mechanical stimulus, noted as "mech"). Inserts represent magnified nuclear membrane at locations specified with arrows. Scale bars in time-lapse images and inserts represent 5 μm and 1 μm, respectively.

E) Change in lifetime at different ROIs: ER, nucleus membrane (Nuc-mem) and indentation site ("Indent-site") when mechanochemically challenged by either CytoD or Control using pyramidal (top row) and cylindrical (bottom row) probes (Mean ± SD, $N \geq 3$, $n \geq 11$, ***$p < 0.001$, **$p < 0.01$, *$p < 0.05$, reported p-values of $0.05 \leq p < 0.1$, t-test). Orange arrows indicate the injection pulse at the specified time in the mechanochemical process.

F) Box plots showing lifetime change upon retracting probes from the injected cells at different ROIs: ER, Nuc-mem and indentation site. Mean values are shown with triangles ($N \geq 3$, $n \geq 11$, ***$p < 0.001$, **$p < 0.01$, *$p < 0.05$, reported p-values of $0.05 \leq p < 0.1$, ns: not significant, t-test).

G) Schematic represents the tension report of ER Flipper-TR dye inside the membrane of the nucleus and the ER before (left panel) and after mechanochemical triggering of the nucleus with DMSO (as control, middle panel) or CytoD (right panel). In contrast to control cells, delivery of CytoD induces more accumulated tension (i.e., FLIM data) at the nuclear membrane and the ER because it disrupts load-bearing actin component of cytoskeleton. ONM: outer nuclear membrane, INM: inner nuclear membrane, PNS: perinuclear space, and σ: tension exerted by indenting the nucleus using FluidFM probes.

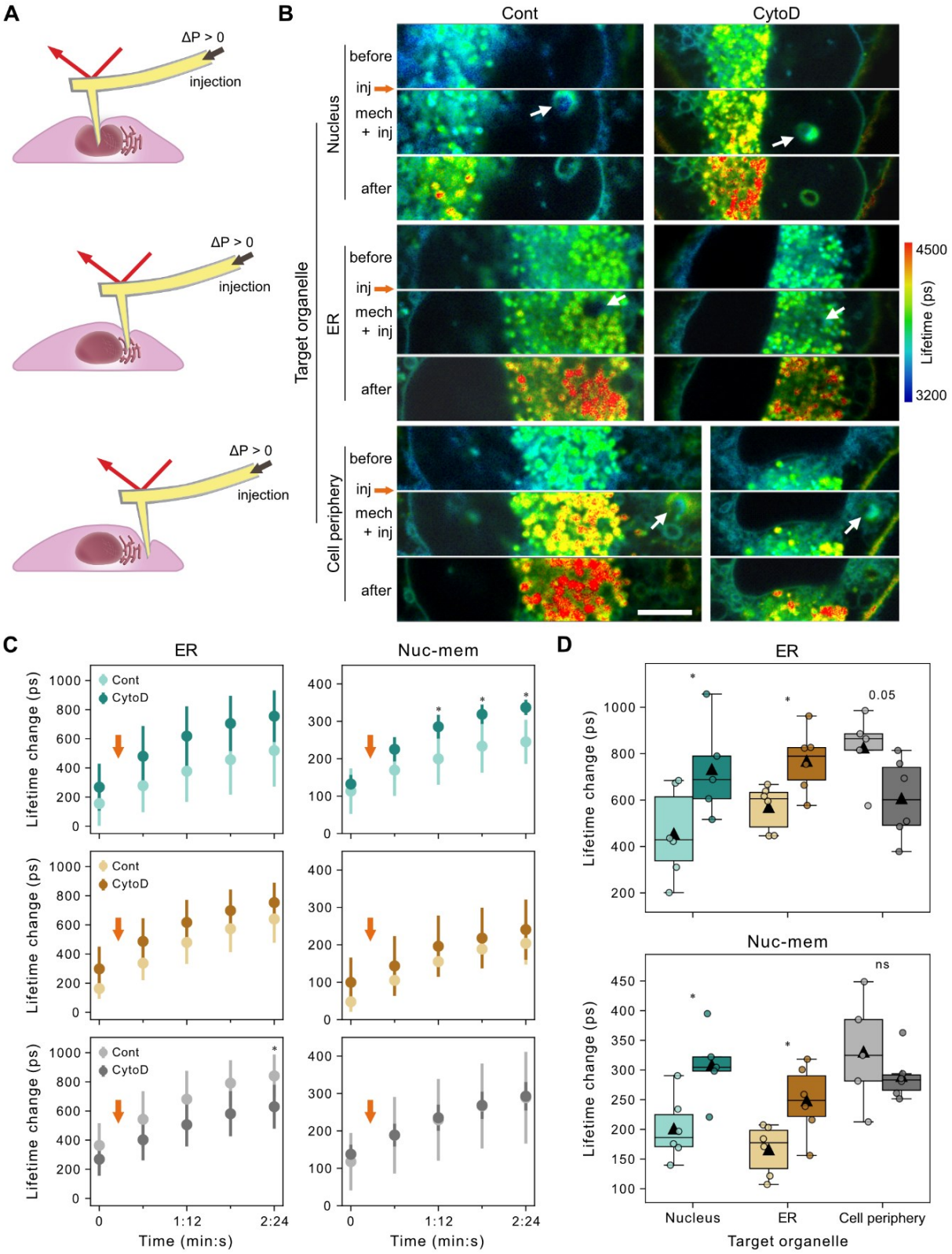

Fig. 3. ER and nuclear envelope crosstalk as a response to mechanochemical triggering of different intracellular components of HeLa cells.

A) Schematic shows targeting different organelles for mechanochemical stimulation: nucleus (top), the ER (middle) and cell periphery (bottom).

B) Lifetime images of HeLa cells stained with the ER Flipper-TR before, at mechanochemical stimulated state ("mech + inj") and after stimulation targeting different subcellular compartments: nucleus (top panel), the ER (middle panel) and cell periphery (bottom panel) for indentation and injection of either control (Cont) or CytoD using sharpened cylindrical probes. Arrows indicate where the cylindrical probe penetrates the cell ("Indent-site"). Scale bar represents 5 μm.

C, D) Change in lifetime at the ER and nucleus membrane (Nuc-mem) during (C, noted as "mech + inj" in B) and after (D) stimuli imposing injection of DMSO as control (light) or CytoD (dark) at different subcellular compartments: nucleus (top panel), ER (middle panel) and cell periphery (bottom panel) (Mean ± SD, $N = 2$, $n \geq 5$, $^{**}p < 0.01$, $^{*}p < 0.05$, t-test). Orange arrows in C indicate the injection pulse at the specified time in the mechanochemical process. Mean values are shown with triangles in boxplots in D ($N = 2$, $n \geq 5$, $^{*}p < 0.05$, reported p-values of $0.05 \leq p < 0.1$, ns: not significant, t-test).

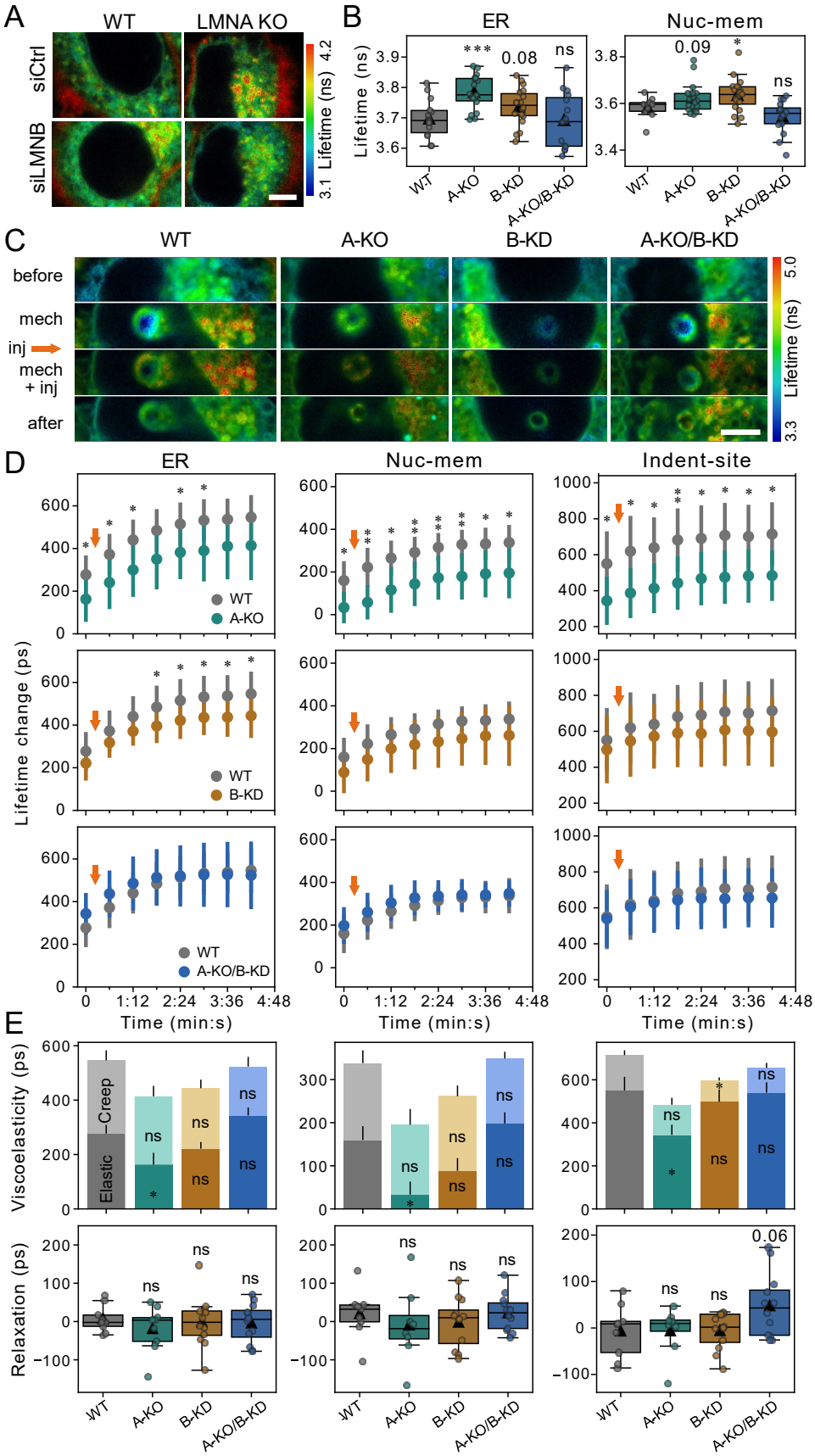
A
WT
LMNA KO
siCtrl
siLMNB
Lifetime (ns)
4.2
3.1
B
ER
Nuc-mem
Lifetime (ns)
***
0.08
ns
0.09
*
ns
WT
A-KO
B-KD
A-KO/B-KD
C
WT
A-KO
B-KD
A-KO/B-KD
before
mech
inj
mech + inj
after
Lifetime (ns)
5.0
3.3
D
ER
Nuc-mem
Indent-site
Lifetime change (ps)
WT
A-KO
B-KD
A-KO/B-KD
Time (min:s)
0
1:12
2:24
3:36
4:48
E
Viscoelasticity (ps)
Creep
Elastic
Relaxation (ps)
ns
0.06
WT
A-KO
B-KD
A-KO/B-KD

Fig. 4. A-type lamins contribute to elasticity, while B-type lamins may influence viscosity in the nucleus's viscoelastic behavior under sustained deformation with disrupted actin polymerization.

A, B) Lifetime images (A) and boxplots showing the absolute lifetime values (B) of HeLa cells with varied levels of downregulation of lamin proteins: WT-siCtrl (WT), WT-siLMNB (A-KO), LMNA KO-siLMNB (B-KD) and LMNA KO-siLMNB (A-KO/B-KD). Cells were stained with ER Flipper-TR dye. Scale bar in A represents 5 μm. Mean values are shown with triangles in B ($N = 2$, $n \geq 8$, ***$p < 0.001$, *$p < 0.05$, reported p-values of $0.05 \leq p < 0.1$, ns: not significant, t-test).

C) Lifetime images of WT, A-KO, B-KD and A-KO/B-KD cells stained with ER Flipper-TR before, upon indentation ("mech"), upon indentation + CytoD injection, "mech + inj", and after stimulation using sharpened cylindrical probes. Note the extended range for lifetime, compared to A, revealing distinguished cell responses to the stimuli, thus indicating the initial tension state for different cell versions in the same color. Scale bar represents 5 μm.

D) Lifetime change at the ER, nucleus membrane (Nuc-mem) and indentation site during mechanochemical stimuli. All cells were injected with CytoD. In each panel, the tension response of WT cells were compared with either of A-KO, B-KD and A-KO/B-KD cells. Orange arrows indicate the injection pulse at the specified time in the mechanochemical process. Time zero corresponds to the indented state (indicated by "mech" in C) which follows by an injection (indicated by "mech + inj" in C) (Mean ± SD, $N = 3$, $n \geq 9$).

E, top) Viscoelastic response of cell compartments (left to right: ER, Nuc-mem and Indent-site) with varied depletion of lamins to the mechanochemical stimuli composed of lifetime change originating from the instantaneous cell response (Elastic) upon indentation in nucleus (first time points in D) and from the time-dependent response (Creep) due to AFM probe being in contact with the nucleus (at 150 nN) for around 4 min after CytoD injection (last time points in D). Data represent the mean ± SEM ($N = 3$, $n \geq 9$, ***$p < 0.001$, **$p < 0.01$, *$p < 0.05$, reported p-values of $0.05 \leq p < 0.1$, t-test). **E, bottom)** Relaxation behavior of WT, A-KO, B-KD and A-KO/B-KD cells at varied positions (left to right: ER, Nuc-mem and Indent-site) after stimuli reported as lifetime change right after probe retraction compared to last time point during stimuli (last time points in D). Mean values are shown with triangles in boxplots ($N = 3$, $n \geq 9$, reported p-values of $0.05 \leq p < 0.1$, ns: not significant, t-test).

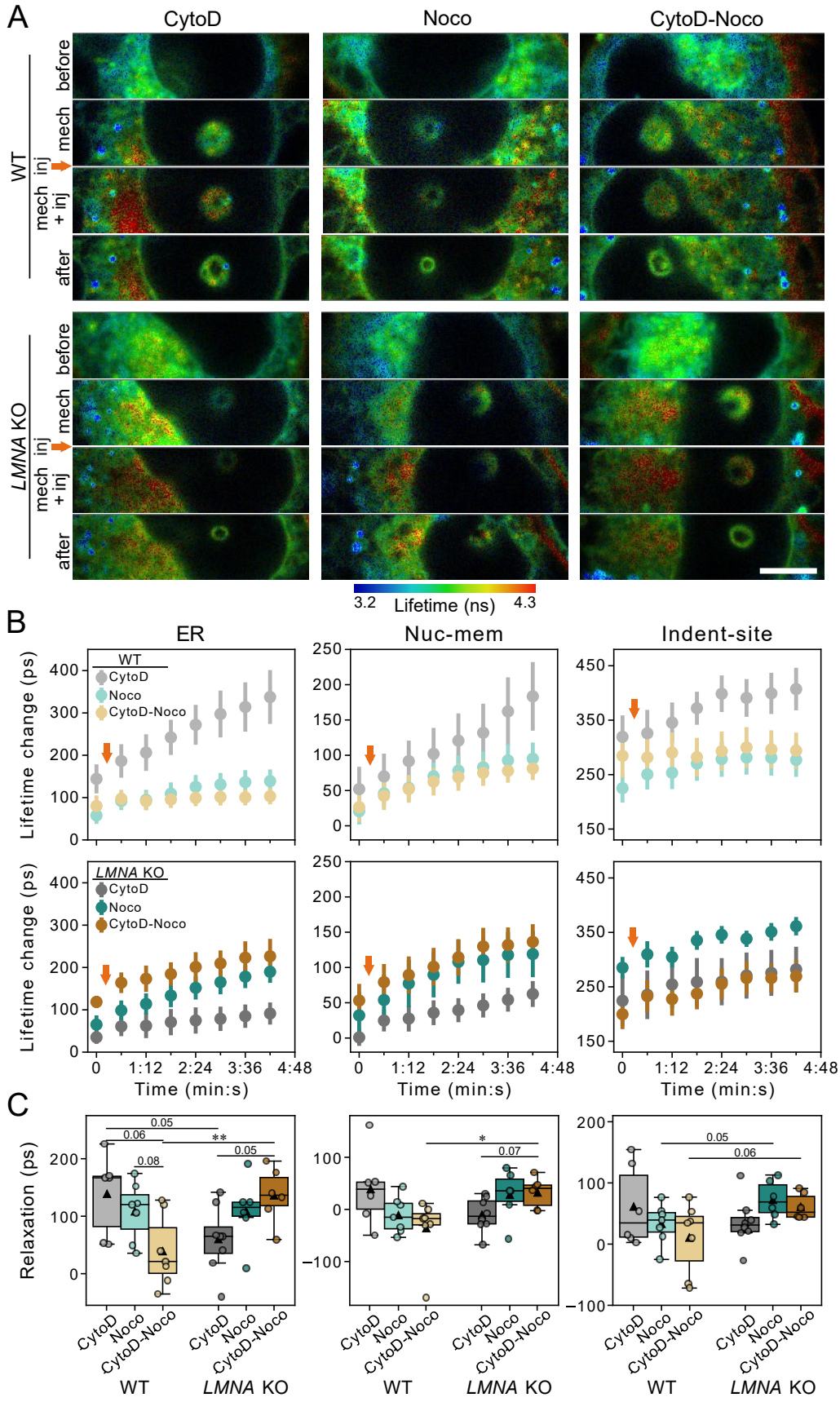
A
CytoD
Noco
CytoD-Noco
WT
before
mech inj
mech inj + inj
after
LMNA KO
before
mech inj
mech inj + inj
after
3.2
Lifetime (ns)
4.3
B
ER
Nuc-mem
Indent-site
WT
CytoD
Noco
CytoD-Noco
LMNA KO
CytoD
Noco
CytoD-Noco
Lifetime change (ps)
Time (min:s)
0
1:12
2:24
3:36
4:48
C
Relaxation (ps)
0.05
0.06
0.08
**
0.05
*
0.07
0.05
0.06
CytoD
Noco
CytoD-Noco
WT
LMNA KO

Fig. 5. Dynamic role of microtubules and actinomyosin in regulating mechanoresponse of nuclei in cells with and without lamin A/C-depletion to the external stimulus.

A) Lifetime images of WT- and LMNA KO-HeLa cells stained with ER Flipper-TR before, upon indentation ("mech"), upon indentation + injection ("mech + inj") of various drugs and after stimulation using sharpened cylindrical probes. For chemical stimulation, interruption of different cytoskeleton components including actin filaments, microtubules and both of actin filaments and microtubules was targeted realized by injection of 50 μM CytoD (left column), 50 μM Noco (middle column) and 50μM CytoD + 50μM Noco (right column) dissolved in DMSO. Scale bar represents 5 μm.

B) Lifetime change at ER, nucleus membrane (Nuc-mem) and indentation site during stimuli in WT and LMNA KO cells. Arrows indicate the injection pulse at the specified time in the mechanochemical process. Time zero corresponds to indented state (indicated by "mech" in A) which follows by injection, indicated by "mech + inj" in A (Mean ± SEM, N = 2, n ≥ 6, **p <0.01, *p < 0.05, reported p-values of 0.05 ≤ p < 0.1, t-test with Holm correction).

C) Relaxation behavior of WT and LMNA KO cells at varied positions (left to right: ER, Nuc-mem and Indent-site) 5 min after mechanochemical stimuli involving various drugs (CytoD, Noco and CytoD-Noco). Relaxation is reported as lifetime change at 5 min after probe retraction compared to the last time point of stimuli (last time points in B). Mean values are shown with triangles in boxplots (N = 2, n ≥ 6, **p <0.01, *p < 0.05, reported p-values of 0.05 ≤ p < 0.1, t-test with Holm correction).